We are IntechOpen,
the world's leading publisher of
Open Access books
Built by scientists, for scientists

6,900
Open access books available

185,000
International authors and editors

200M
Downloads

Our authors are among the

154
Countries delivered to

TOP 1%
most cited scientists

12.2%
Contributors from top 500 universities

CLARIVATE ANALYTICS

BOOK CITATION INDEX

INDEXED

WEB OF SCIENCE™

Selection of our books indexed in the Book Citation Index
in Web of Science™ Core Collection (BKCI)

Interested in publishing with us?
Contact book.department@intechopen.com

Numbers displayed above are based on latest data collected.
For more information visit www.intechopen.com

About array processing methods for image segmentation

J. Marot, C. Fossati
Institut Fresnel (Ecole Centrale Marseille)
France
Y. Caulier
Fraunhofer Institute IIS
Germany

1. Introduction

Shape description is an important goal of computational vision and image processing. Giving the characteristics of lines or distorted contours is faced in robotic way screening, measuring of wafer track width in microelectronics, aerial image analysis, vehicle trajectory and particle detection. Distorted contour retrieval is also encountered in medical imaging. In this introduction, we firstly present classical methods that were proposed to solve this problem, that is, Snakes and levelset methods (Kass et al., 1988; Xu & Prince, 1997; Zhu & Yuile, 1996; Osher & Sethian, 1988; Paragios & Deriche, 2002). We secondly present original methods which rely on signal generation out of an image and adaptation of high resolution methods of array processing (Aghajan & Kailath, 1993a; Aghajan, 1995; Bourennane & Marot, 2006; Marot & Bourennane, 2007a; Marot & Bourennane, 2007b; Marot & Bourennane, 2008).

A Snake is a closed curve which, starting from an initial position, evolves towards an object of interest under the influence of forces (Kass et al., 1988; Xu & Prince, 1997; Zhu & Yuile, 1996; Xianhua & Mirmehdi, 2004; Cheng & Foo 2006; Brigger et al., 2000) Snakes methods are edge-based segmentation schemes which aim at finding out the transitions between uniform areas, rather than directly identifying them (Kass et al., 1988; Xu & Prince, 1997). Another model of active contour is geodesic curves or "levelset". Its main interest with respect to Snakes is to be able to face changes in topology, to the cost of a higher computational load (Osher & Sethian, 1988; Paragios & Deriche 2002; Karoui et al., 2006).

We describe here more precisely Snakes type methods because they are edge-based methods as well as the proposed array processing methods. Edge-based segmentation schemes have improved, considering robustness to noise and sensitivity to initialization (Xu & Prince, 1997). Some active contour methods were combined with spline type interpolation to reduce the number of control points in the image (Brigger et al. 2000). This increases the robustness to noise and computational load. In particular, (Precioso et al., 2005) uses smoothing splines in the B-spline interpolation approach of (Unser et al. 1993). In (Xu & Prince, 1997) the proposed "Gradient Vector Flow" (GVF) method provides valuable results, but is prone to

shortcomings: contours with high curvature may be skipped unless an elevated computational load is devoted. Concerning straight lines in particular, in (Kiryati & Brucktein, 1992; Sheinval & Kiryati, 1997) the extension of the Hough transform retrieves the main direction of roughly aligned points. This method gives a good resolution even with noisy images. Its computational load is elevated. Least-squares fit of straight lines seeks to minimize the summation of the squared error-of-fit with respect to measures (Gander et al., 1994; Connel & Jain, 2001). This method is sensitive to outliers.

An original approach in contour estimation consists in adapting high-resolution methods of array processing (Roy & Kailath, 1989; Pillai & Kwon, 1989; Marot et al., 2008) for straight line segmentation (Aghajan & Kailath, 1993a; Aghajan, 1995; Aghajan & Kailath, 1993b; Halder et al., 1995; Aghajan & Kailath, 1994; Aghajan & Kailath, 1992). In this framework, a straight line in an image is considered as a wave-front. Now, high-resolution methods of array processing have improved for several years (Roy & Kailath, 1989; Bourennane et al., 2008). In particular, sensitivity to noise has improved, and the case of correlated sources is faced by a "spatial smoothing" procedure (Pillai & Kwon 1989). To adapt high-resolution methods of array processing to contour estimation in images, the image content is transcripted into a signal through a specific generation scheme, performed on a virtual set of sensors located along the image side. In (Abed-Meraim & Hua, 1997), a polynomial phase model for the generated signal is proposed to take into account the image discretization, for an improved straight line characterization. The ability of high-resolution methods to handle correlated sources permitted to handle the case of parallel straight lines in image understanding (Bourennane & Marot, 2006; Bourennane & Marot, 2005). Optimization methods generalized straight line estimation to nearly straight distorted contour estimation (Bourennane & Marot, 2005; Bourennane & Marot, 2006b; Bourennane & Marot, 2006c).

Circular and nearly circular contour segmentation (Marot & Bourennane, 2007a; Marot & Bourennane, 2007b) was also considered. While straight and nearly straight contours are estimated through signal generation on linear antenna, circular and nearly circular contour segmentation is performed through signal generation upon circular antenna. We adapt the shape of the antenna to the shape of the expected contours so we are able to apply the same high-resolution and optimization methods as for straight and nearly straight line retrieval. In particular array processing methods for star-shaped contour estimation provide a solution to the limitation of Snakes active contours concerning contours with high concavity (Marot & Bourennane, 2007b). The proposed multiple circle estimation method retrieves intersecting circles, thus providing a solution to levelset-type methods.

The remainder of the chapter is organized as follows: We remind in section 2 the formalism that adapts the estimation of straight lines as a classical array processing problem. The study dedicated to straight line retrieval is used as a basis for distorted contour estimation (see section 3). In section 4 we set the problem of star-shaped contour retrieval and propose a circular antenna to retrieve possibly distorted concentric circles. In section 5 we summarize the array processing methods dedicated to possibly distorted linear and circular contour estimation. We emphasize the similarity between nearly linear and nearly circular contour estimation. In section 6 we show how signal generation on linear antenna yields the coordinates of the center of circles. In section 7 we describe a method for the estimation of intersecting circles, thereby proposing a solution to a limitation of the levelset type algorithms. In section 8 we propose some results through various applications: robotic vision, omni directional images, and medical melanoma images.

2. Straight contour estimation

2.1 Data model, generation of the signals out of the image data

To adapt array processing techniques to distorted curve retrieval, the image content must be transcripted into a signal. This transcription is enabled by adequate conventions for the representation of the image, and by a signal generation scheme (Aghajan, 1995; Aghajan & Kailath, 1994). Once a signal has been created, array processing methods can be used to retrieve the characteristics of any straight line. Let I be the recorded image (see Fig.1 (a).).
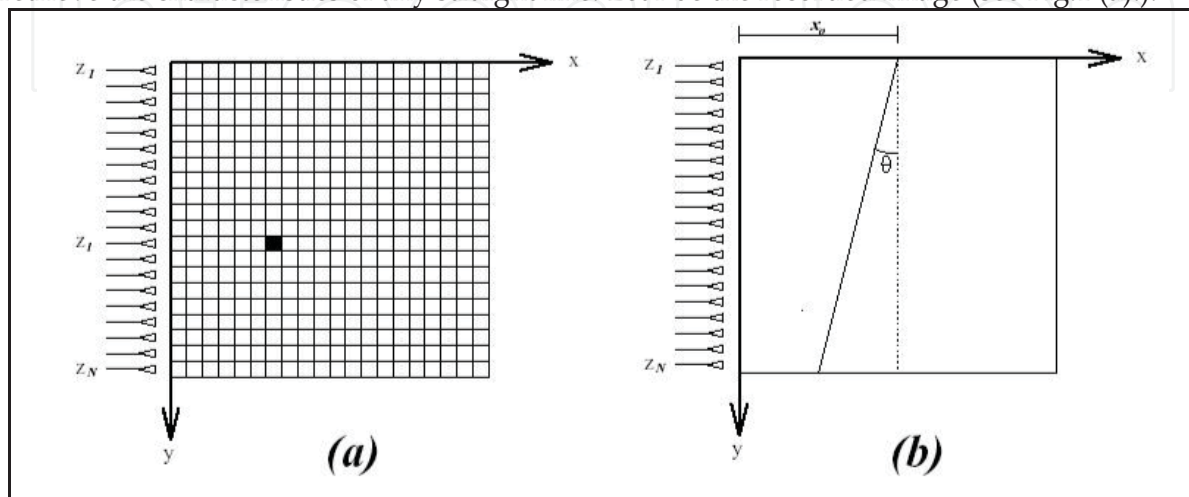
Fig. 1. The image model (see Aghajan & Kailath, 1992):

(a) The image-matrix provided with the coordinate system and the linear array of N equidistant sensors,
(b) A straight line characterized by its angle θ and its offset x_0.

We consider that I contains d straight lines and an additive uniformly distributed noise. The image-matrix is the discrete version of the recorded image, compound of a set of $N * C$ pixel values. A formalism adopted in (Aghajan & Kailath, 1993) allows signal generation, by the following computation:

$$z(i) = \sum_{k=1}^{C} I(i,k)\,exp(-j\mu k), \quad i = 1,\dots\dots,N \tag{1}$$

Where $\left\{I(i,k); i \in \{1,\dots,N\}; k \in \{1,\dots,C\}\right\}$ denote the image pixels. Eq. (1) simulates a linear antenna: each row of the image yields one signal component as if it were associated with a sensor. The set of sensors corresponding to all rows forms a linear antenna. We focus in the following on the case where a binary image is considered. The contours are composed of 1-valued pixels also called "edge pixels", whereas 0-valued pixels compose the background. When d straight lines, with parameters angle $\{\theta_k\}$ and offset $x_{0k}\,(k = 1,\dots,d)$, are crossing the image, and if the image contains noisy outlier pixels, the signal generated on the ith sensor, in front of the ith row, is (Aghajan & Kailath, 1993):

$$z(i) = \sum_{k=1}^{d} exp\,(j\mu(i-1)\,tan(\theta_k))\,exp(-j\mu x_{0k}) + n(i) \tag{2}$$

Where μ is a propagation parameter (Aghajan & Kailath, 1993b) and $n(i)$ is due to the noisy pixels on the ith row.

Defining $a_i(\theta_k) = exp(j\mu(i-1)tan\,\theta_k)$, $s_k = exp(-j\mu x_{0k})$, Eq. (2) becomes:

$$z(i) = \sum_{k=1}^{d} a_i(\theta_k)s_k + n(i), \quad i = 1,...,N \tag{3}$$

Grouping all terms in a single vector, Eq. (3) becomes:

$\mathbf{z} = \mathbf{A}(\theta)\mathbf{s} + \mathbf{n}$, with $\mathbf{A}(\theta) = [\mathbf{a}(\theta_1),...,\mathbf{a}(\theta_d)]$ where $\mathbf{a}(\theta_k) = [a_1(\theta_k), a_2(\theta_k),...,a_N(\theta_k)]^T$, with $a_i(\theta_k) = exp(j\mu(i-1)tan\,\theta_k)$, $i = 1,...,N$, superscript T denoting transpose. SLIDE (Subspace-based Line DEtection) algorithm (Aghajan & Kailath, 1993) uses TLS-ESPRIT (Total-Least-Squares Estimation of Signal Parameters via Rotational Invariance Techniques) method to estimate the angle values.

To estimate the offset values, the "extension of the Hough transform" (Kiryati & Bruckstein, 1992) can be used. It is limited by its high computational cost and the large required size for the memory bin. (Bourennane & Marot, 2006a; Bourennane & Marot, 2005) developed another method. This method remains in the frame of array processing and reduces the computational cost: A high-resolution method called MFBLP (Modified Forward Backward Linear Prediction) (Bourennane & Marot, 2005) is associated with a specific signal generation method, namely the variable parameter propagation scheme (Aghajan & Kailath, 1993b). The formalism introduced in that section can also handle the case of straight edge detection in gray-scale images (Aghajan & Kailath, 1994).

In the next section, we consider the estimation of the straight line angles and offsets, by reviewing the SLIDE and MFBLP methods.

2.2 Angle estimation, overview of the SLIDE method

The method for angles estimation falls into two parts: the estimation of a covariance matrix and the application of a total least squares criterion.

Numerous works have been developed in the frame of the research of a reliable estimator of the covariance matrix when the duration of the signal is very short or the number of realizations is small. This situation is often encountered, for instance, with seismic signals. To cope with it, numerous frequency and/or spatial means are computed to replace the temporal mean. In this study the covariance matrix is estimated by using the spatial mean (Halder & al., 1995). From the observation vector we build K vectors of length M with $d < M \leq N-d+1$. In order to maximize the number of sub-vectors we choose $K=N+1-M$. By grouping the whole sub-vectors obtained in matrix form, we obtain : $\mathbf{Z}_K = [\mathbf{z}_1,...,\mathbf{z}_K]$, where $\mathbf{z}_l = \mathbf{A}_M(\theta)\mathbf{s}_l + \mathbf{n}_l$, $l = 1,...,K$. Matrix $\mathbf{A}_M(\theta) = [\mathbf{a}(\theta_1),...,\mathbf{a}(\theta_d)]$ is a Vandermonde type one of size M x d. Signal part of the data is supposed to be independent from the noise; the components of noise vector $\mathbf{n}_l$ are supposed to be uncorrelated, and to have identical variance. The covariance matrix can be estimated from the observation sub-vectors as it is performed in (Aghajan & Kailath, 1992). The eigen-decomposition of the covariance matrix is, in general, used to characterize the sources by subspace techniques in array processing. In the frame of image processing the aim is to estimate the angle θ of the d straight lines. Several high-resolution methods that solve this problem have been proposed (Roy & Kailath, 1989). SLIDE algorithm is applied to a particular case of an array consisting of two

identical sub-arrays (Aghajan & Kailath, 1994). It leads to the following estimated angles (Aghajan & Kailath, 1994):

$$\hat{\theta}_k = tan^{-1}\left[\frac{1}{(\mu * \Delta)} Im\left(ln\left(\frac{\lambda_k}{|\lambda_k|}\right)\right)\right] \tag{4}$$

where $\{\lambda_k, k = 1,...,d\}$ are the eigenvalues of a diagonal unitary matrix that relates the measurements from the first sub-array to the measurements resulting from the second sub-array. Parameter μ is the propagation constant, and Δ is the distance between two sensors. TLS-ESPRIT method used by SLIDE provides the estimated parameters in closed-form, in opposite to the Hough transform which relies on maxima research (Kiryati & Bruckstein, 1992). Offset estimation exploits the estimated straight lines angles.

2.3 Offset estimation

The most well-known offset estimation method is the "Extension of the Hough Transform" (Sheinvald & Kiryati, 1997). Its principle is to count all pixel aligned on several orientations. The expected offset values correspond to the maximum pixel number, for each orientation value. The second proposed method remains in the frame of array processing: it employs a variable parameter propagation scheme (Aghajan, 1993; Aghajan & Kailath, 1993b; Aghajan & Kailath, 1994) and uses a high resolution method. This high resolution "MFBLP" method relies on the concept of forward and backward organization of the data (Pillai & Kwon, 1989; Halder, Aghajan et al., 1995; Tufts & Kumaresan, 1982). A variable speed propagation scheme (Aghajan & Kailath, 1993b; Aghajan & Kailath, 1994), associated with "MFBLP" (Modified Forward Backward Linear Prediction) yields offset values with a lower computational load than the Extension of the Hough Transform. The basic idea in this method is to associate a propagation speed which is different for each line in the image (Aghajan & Kailath, 1994). By setting artificially a propagation speed that linearly depends on row indices, we get a linear phase signal. When the first orientation value is considered, the signal received on sensor i $(i = 1,...N)$ is then:

$$z(i) = \sum_{k=1}^{d_1} exp(-j\tau x_{0k}) exp(j\tau(i-1)tan(\theta_1)) + n(i) \tag{5}$$

d_1 is the number of lines with angle θ_1. When τ varies linearly as a function of the line index the measure vector **z** contains a modulated frequency term. Indeed we set $\tau = \alpha(i-1)$.

$$z(i) = \sum_{k=1}^{d_1} exp(-j\alpha(i-1)x_{0k}) exp(j\alpha(i-1)^2 tan(\theta_1)) + n(i) \tag{6}$$

This is a sum of d_1 signals that have a common quadratic phase term but different linear phase terms. The first treatment consists in obtaining an expression containing only linear terms. This goal is reached by dividing *z(i)* by the non zero term $a_i(\theta_1) = exp(j\alpha(i-1)^2 tan(\theta_1))$. We obtain then:

$$w(i) = \sum_{k=1}^{d_1} exp\left(-j\alpha(i-1)x_{0k}\right) + n'(i) \tag{7}$$

The resulting signal appears as a combination of d_1 sinusoids with frequencies:

$$f_k = \frac{\alpha x_{0k}}{2\pi}, \quad k = 1,...,d_1 \tag{8}$$

Consequently, the estimation of the offsets can be transposed to a frequency estimation problem. Estimation of frequencies from sources having the same amplitude was considered in (Tufts & Kumaressan, 1982). In the following a high resolution algorithm, initially introduced in spectral analysis, is proposed for the estimation of the offsets.

After adopting our signal model we adapt to it the spectral analysis method called modified forward backward linear prediction (MFBLP) (Tufts & Kumaresan, 1982) for estimating the offsets: we consider d_k straight lines with given angle θ_k, and apply the MFBLP method, to the vector $\mathbf{w}$. Details about MFBLP method applied to offset estimation are available in (Bourennane & Marot, 2006a). MFBLP estimates the values of f_k, $k = 1,...,d_1$. According to Eq. (8) these frequency values are proportional to the offset values, the proportionality coefficient being $-\alpha$. The main advantage of this method comes from its low computational load. Indeed the complexity of the variable parameter propagation scheme associated with MFBLP is much less than the complexity of the Extension of the Hough Transform as soon as the number of non zero pixels in the image increases. This algorithm enables the characterization of straight lines with same angle and different offset.

3. Nearly linear contour retrieval

In this section, we keep the same signal generation formalism as for straight line retrieval. The more general case of distorted contour estimation is proposed. The reviewed method relies on constant speed signal generation scheme, and on an optimization method.

3.1 Initialization of the proposed algorithm

To initialize our recursive algorithm, we apply SLIDE algorithm, which provides the parameters of the straight line that fits the best the expected distorted contour. In this section, we consider only the case where the number d of contours is equal to one. The parameters angle and offset recovered by the straight line retrieval method are employed to build an initialization vector $\mathbf{x_0}$, containing the initialization straight line pixel positions:

$$\mathbf{x_0} = \left[x_0, x_0 - tan(\theta),..., x_0 - (N-1)tan(\theta)\right]^T$$

Fig.2 presents a distorted curve, and an initialization straight line that fits this distorted curve.
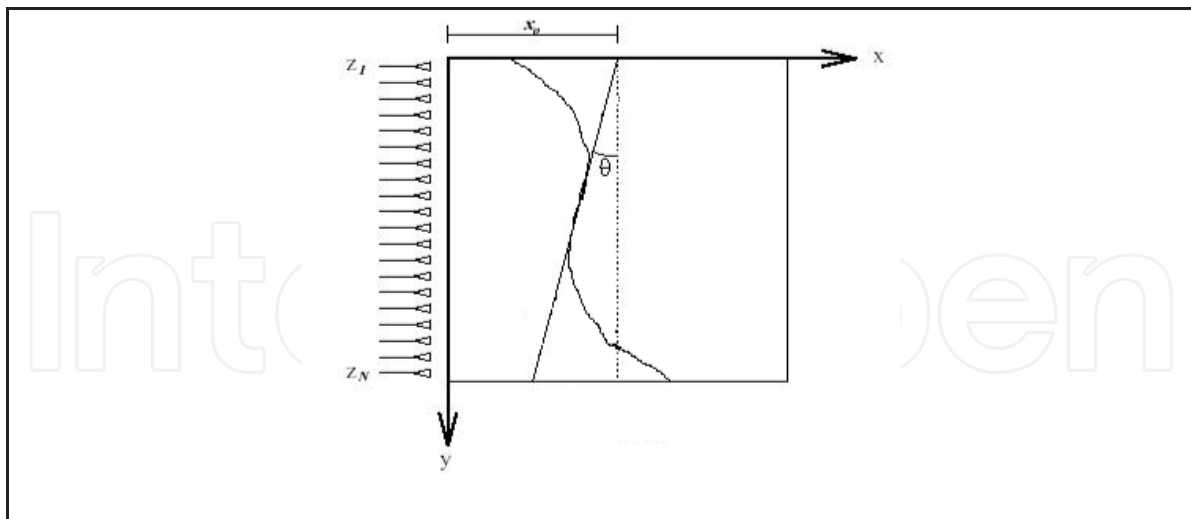
Fig. 2. A model for an image containing a distorted curve

3.2 Distorted curve: proposed algorithm

We aim at determining the N unknowns $x(i)$, $i = 1,...,N$ of the image, forming a vector $\mathbf{x_{input}}$, each of them taken into account respectively at the ith sensor:

$$z(i) = exp(-j\mu x(i)), \quad \forall i = 1,...,N \tag{9}$$

The observation vector is

$$\mathbf{z_{input}} = [exp(-j\mu x(1)),...,exp(-j\mu x(N))]^T \tag{10}$$

We start from the initialization vector $\mathbf{x_0}$, characterizing a straight line that fits a locally rectilinear portion of the expected contour. The values $x(i)$, $i = 1,...,N$ can be expressed as: $x(i) = x_0 - (i-1)tan(\theta) + \Delta x(i)$, $i = 1,...,N$ where $\Delta x(i)$ is the pixel shift for row i between a straight line with parameters θ and the expected contour. Then, with k indexing the steps of this recursive algorithm, we aim at minimizing

$$J(\mathbf{x_k}) = \|\mathbf{z_{input}} - \mathbf{z_{estimated\ for\ x_k}}\|^2 \tag{11}$$

where $\|.\|$ represents the C^N norm. For this purpose we use fixed step gradient method:

$\forall k \in N: \mathbf{x_{k+1}} = \mathbf{x_k} - \lambda \nabla(J(\mathbf{x_k}))$, λ is the step for the descent. At this point, by minimizing criterion J (see Eq. (11)), we find the components of vector $\mathbf{x}$ leading to the signal $\mathbf{z}$ which is the closest to the input signal in the sense of criterion J. Choosing a value of μ which is small enough (see Eq. (1)) avoids any phase indetermination. A variant of the fixed step gradient method is the variable step gradient method. It consists in adopting a descent step which depends on the iteration index. Its purpose is to accelerate the convergence of gradient. A more elaborated optimization method based on DIRECT algorithm (Jones et al., 1993) and spline interpolation (Marot & Bourennane, 2007a) can be adopted to reach the global minimum of criterion J of Eq. (11). This method is applied to modify recursively signal $\mathbf{z_{estimated\ for\ x_k}}$: at each step of the recursive procedure vector $\mathbf{x_k}$ is computed by making an interpolation between some "node" values that are retrieved by DIRECT. The

interest of the combination of DIRECT with spline interpolation comes from the elevated computational load of DIRECT. Details about DIRECT algorithm are available in (Jones et al., 1993). Reducing the number of unknown values retrieved by DIRECT reduces drastically its computational load. Moreover, in the considered application, spline interpolation between these node values provides a continuous contour. This prevents the pixels of the result contour from converging towards noisy pixels. The more interpolation nodes, the more precise the estimation, but the slower the algorithm.

After considering linear and nearly linear contours, we focus on circular and nearly circular contours.

4. Star-shape contour retrieval

Star-shape contours are those whose radial coordinates in polar coordinate system are described by a function of angle values in this coordinate system. The simplest star-shape contour is a circle, centred on the origin of the polar coordinate system.

Signal generation upon a linear antenna yields a linear phase signal when a straight line is present in the image. While expecting circular contours, we associate a circular antenna with the processed image. By adapting the antenna shape to the shape of the expected contour, we aim at generating linear phase signals.

4.1 Problem setting and virtual signal generation

Our purpose is to estimate the radius of a circle, and the distortions between a closed contour and a circle that fits this contour. We propose to employ a circular antenna that permits a particular signal generation and yields a linear phase signal out of an image containing a quarter of circle. In this section, center coordinates are supposed to be known, we focus on radius estimation, center coordinate estimation is explained further. Fig. 3(a) presents a binary digital image I. The object is close to a circle with radius value r and center coordinates (l_c, m_c). Fig. 3(b) shows a sub-image extracted from the original image, such that its top left corner is the center of the circle. We associate this sub-image with a set of polar coordinates (ρ, θ), such that each pixel of the expected contour in the sub-image is characterized by the coordinates $(r + \Delta\rho, \theta)$, where $(\Delta\rho)$ is the shift between the pixel of the contour and the pixel of the circle that roughly approximates the contour and which has same coordinate θ. We seek for star-shaped contours, that is, contours that can be described by the relation: $\rho = f(\theta)$ where f is any function that maps $[0, 2\pi]$ to R_+. The point with coordinate $\rho = 0$ corresponds then to the center of gravity of the contour.

Generalized Hough transform estimates the radius of concentric circles when their center is known. Its basic principle is to count the number of pixels that are located on a circle for all possible radius values. The estimated radius values correspond to the maximum number of pixels.
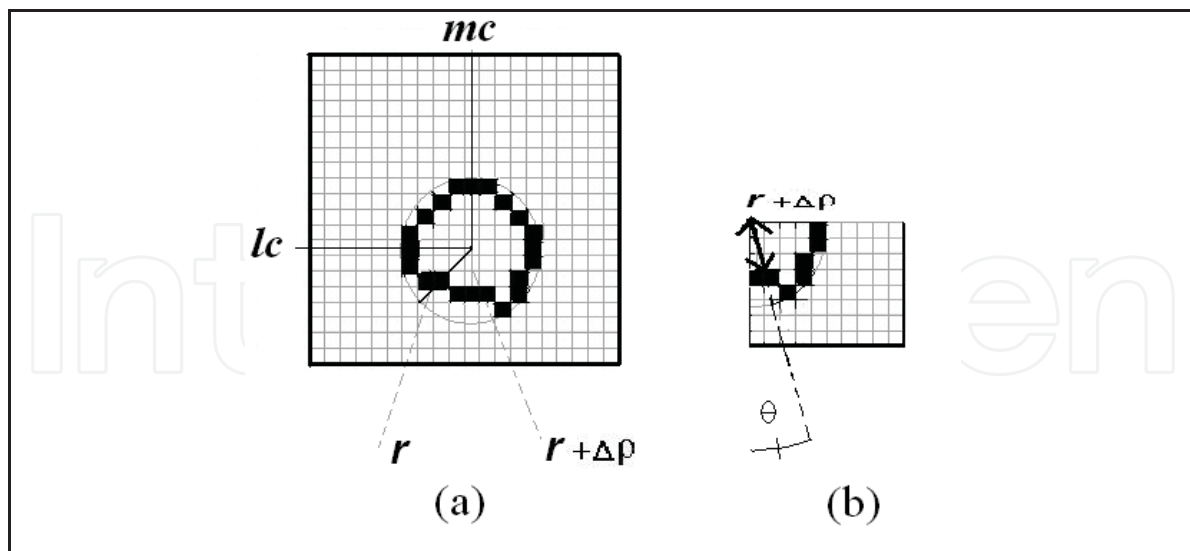
Fig. 3. (a) Circular-like contour, (b) Bottom right quarter of the contour and pixel coordinates in the polar system (ρ,θ) having its origin on the center of the circle. r is the radius of the circle. $\Delta\rho$ is the value of the shift between a pixel of the contour and the pixel of the circle having same coordinate θ

Contours which are approximately circular are supposed to be made of more than one pixel per row for some of the rows and more than one pixel per column for some columns. Therefore, we propose to associate a circular antenna with the image which leads to linear phase signals, when a circle is expected. The basic idea is to obtain a linear phase signal from an image containing a quarter of circle. To achieve this, we use a circular antenna. The phase of the signals which are virtually generated on the antenna is constant or varies linearly as a function of the sensor index. A quarter of circle with radius r and a circular antenna are represented on Fig.4. The antenna is a quarter of circle centered on the top left corner, and crossing the bottom right corner of the sub-image. Such an antenna is adapted to the sub-images containing each quarter of the expected contour (see Fig.4). In practice, the extracted sub-image is possibly rotated so that its top left corner is the estimated center. The antenna has radius R_α so that $R_\alpha = \sqrt{2}N_s$ where N_s is the number of rows or columns in the sub-image. When we consider the sub-image which includes the right bottom part of the expected contour, the following relation holds: $N_s = max(N-l_c, N-m_c)$ where l_c and m_c are the vertical and horizontal coordinates of the center of the expected contour in a cartesian set centered on the top left corner of the whole processed image (see Fig.3). Coordinates l_c and m_c are estimated by the method proposed in (Aghajan, 1995), or the one that is detailed later in this paper.

Signal generation scheme upon a circular antenna is the following: the directions adopted for signal generation are from the top left corner of the sub-image to the corresponding sensor. The antenna is composed of S sensors, so there are S signal components.
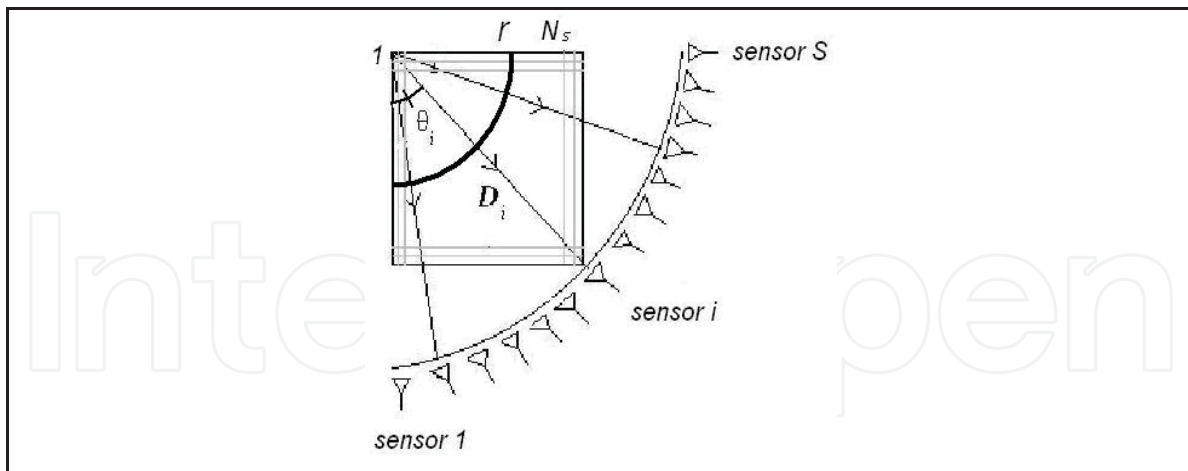
Fig. 4. Sub-image, associated with a circular array composed of S sensors

Let us consider D_i, the line that makes an angle θ_i with the vertical axis and crosses the top left corner of the sub-image. The ith component $(i=1,...,S)$ of the $\mathbf{z}$ generated out of the image reads:

$$z(i) = \sum_{\substack{l,m=1\\(l,m)\in D_i}}^{l,m=N_s} I(l,m)\exp\left(-j\mu\sqrt{l^2+m^2}\right) \tag{12}$$

The integer l (resp. m) indexes the lines (resp. the columns) of the image. j stands for $\sqrt{-1}$. μ is the propagation parameter (Aghajan & Kailath, 1994). Each sensor indexed by i is associated with a line D_i having an orientation $\theta_i = \dfrac{(i-1)\pi/2}{S}$. In Eq. (2), the term (l,m) means that only the image pixels that belong to D_i are considered for the generation of the ith signal component. Satisfying the constraint $(l,m)\in D_i$, that is, choosing the pixels that belong to the line with orientation θ_i, is done in two steps: let *setl* be the set of indexes along the vertical axis, and *setm* the set of indexes along the horizontal axis. If θ_i is less than or equal to $\pi/4$, $setl = [1:N_s]$ and $setm = \lfloor [1:N_s] tan(\theta_i) \rfloor$. If θ_i is greater than $\pi/4$, $setm = [1:N_s]$ and $setl = \lfloor [1:N_s] tan(\pi/2 - \theta_i) \rfloor$. Symbol $\lfloor . \rfloor$ means integer part. The minimum number of sensors that permits a perfect characterization of any possibly distorted contour is the number of pixels that would be virtually aligned on a circle quarter having radius $\sqrt{2}N_s$. Therefore, the minimum number S of sensors is $\sqrt{2}N_s$.

4.2 Proposed method for radius and distortion estimation

In the most general case there exists more than one circle for one center. We show how several possibly close radius values can be estimated with a high-resolution method. For this, we use a variable speed propagation scheme toward circular antenna. We propose a method for the estimation of the number d of concentric circles, and the determination of

each radius value. For this purpose we employ a variable speed propagation scheme (Aghajan & Kailath, 1994). We set $\mu = \alpha(i-1)$, for each sensor indexed by $i = 1,...,S$. From Eq. (12), the signal received on each sensor is:

$$z(i) = \sum_{k=1}^{d} exp(-j\alpha(i-1)r_k) + n(i), \quad i = 1,...,S \tag{13}$$

where $r_k, k = 1,...,d$ are the values of the radius of each circle, and $n(i)$ is a noise term that can appear because of the presence of outliers. All components $z(i)$ compose the observation vector $\mathbf{z}$. TLS-ESPRIT method is applied to estimate $r_k, k = 1,...,d$, the number of concentric circles d is estimated by MDL (Minimum Description Length) criterion. The estimated radius values are obtained with TLS-ESPRIT method, which also estimated straight line orientations (see section 2.2).

To retrieve the distortions between an expected star-shaped contour and a fitting circle, we work successively on each quarter of circle, and retrieve the distortions between one quarter of the initialization circle and the part of the expected contour that is located in the same quarter of the image. As an example, in Fig.3, the right bottom quarter of the considered image is represented in Fig. 3(b). The optimization method that retrieves the shift values between the fitting circle and the expected contour is the following:

A contour in the considered sub-image can be described in a set of polar coordinates by : $\{\rho(i), \theta(i), i = 1,...,S\}$. We aim at estimating the S unknowns $\rho(i), i = 1,...,S$ that characterize the contour, forming a vector:

$$\rho = [\rho(1), \rho(2),...,\rho(S)]^T \tag{14}$$

The basic idea is to consider that ρ can be expressed as: $\rho = [r + \Delta\rho(1), r + \Delta\rho(2),...,r + \Delta\rho(S)]^T$ (see Fig. 3), where r is the radius of a circle that approximates the expected contour.

5. Linear and circular array for signal generation: summary

In this section, we present the outline of the reviewed methods for contour estimation.

An outline of the proposed nearly rectilinear distorted contour estimation method is given as follows:
- Signal generation with constant parameter on linear antenna, using Eq. 1;
- Estimation of the parameters of the straight lines that fit each distorted contour (see subsection 3.1);
- Distortion estimation for a given curve, estimation of $\mathbf{x}$, applying gradient algorithm to minimize a least squares criterion (see Eq. 11).

The proposed method for star-shaped contour estimation is summarized as follows:
- Variable speed propagation scheme upon the proposed circular antenna : Estimation of the number of circles by MDL criterion, estimation of the radius of each circle fitting any expected contour (see Eqs. (12) and (13) or the axial parameters of the ellipse;
- Estimation of the radial distortions, in polar coordinate system, between any expected contour   and the circle or ellipse that fits this contour. Either the

gradient method or the combination of DIRECT and spline interpolation may be used to minimize a least-squares criterion.

Table 1 provides the steps of the algorithms which perform nearly straight and nearly circular contour retrieval. Table 1 provides the directions for signal generation, the parameters which characterize the initialization contour and the output of the optimization algorithm.

	Straight	Circular
Direction for signal generation	row i	$\mathbf{D}_i$
Initialization parameters	θ, x_0	r, center
Pixel shift	$\Delta x(i)$	$\Delta\rho(i)$

Table 1. Nearly straight and nearly circular distorted contour estimation: algorithm steps.

The current section presented a method for the estimation of the radius of concentric circles with *a priori* knowledge of the center. In the next section we explain how to estimate the center of groups of concentric circles.

6. Linear antenna for the estimation of circle center parameters

Usually, an image contains several circles which are possibly not concentric and have different radii (see Fig. 5). To apply the proposed method, the center coordinates for each feature are required. To estimate these coordinates, we generate a signal with constant propagation parameter upon the image left and top sides. The lth signal component, generated from the lth row, reads: $z_{lin}(l) = \sum_{m=1}^{N} I(l,m)exp(-j\mu m)$ where μ is the propagation parameter. The non-zero sections of the signals, as seen at the left and top sides of the image, indicate the presence of features. Each non-zero section width in the left (respectively the top) side signal gives the height (respectively the width) of the corresponding expected feature. The middle of each non-zero section in the left (respectively the top) side signal yields the value of the center l_c (respectively m_c) coordinate of each feature.
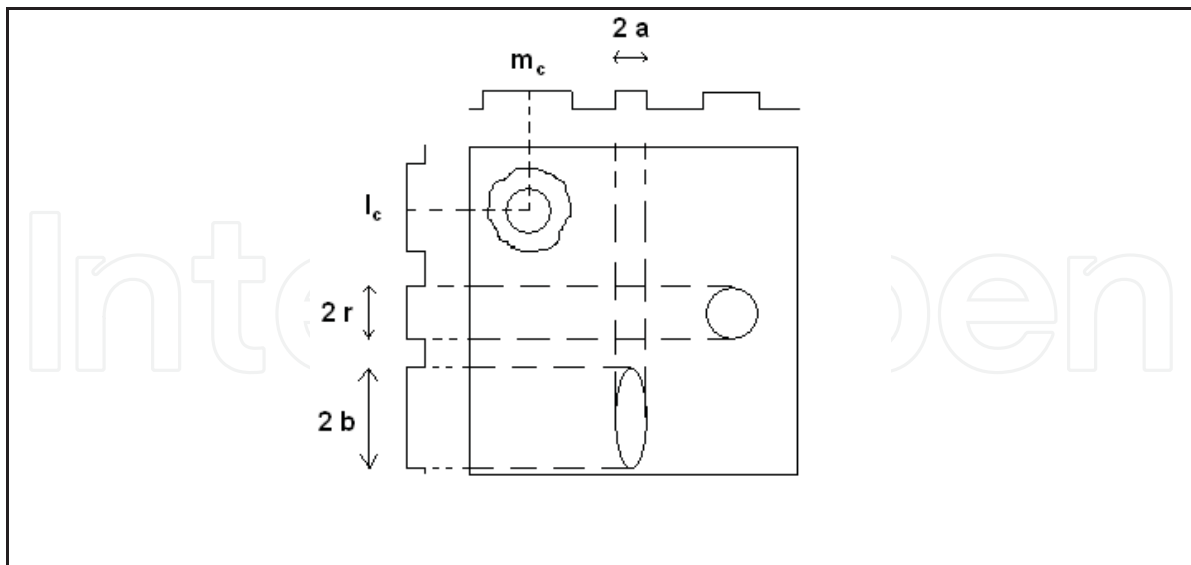
Fig. 5. Nearly circular or elliptic features. *r* is the circle radius, *a* and *b* are the axial parameters of the ellipse.

7. Combination of linear and circular antenna for intersecting circle retrieval

We propose an algorithm which is based on the following remarks about the generated signals. Signal generation on linear antenna yields a signal with the following characteristics: The maximum amplitude values of the generated signal correspond to the lines with maximum number of pixels, that is, where the tangent to the circle is either vertical or horizontal. The signal peak values are associated alternatively with one circle and another. Signal generation on circular antenna yields a signal with the following characteristics: If the antenna is centered on the same center as a quarter of circle which is present in the image, the signal which is generated on the antenna exhibits linear phase properties (Marot & Bourennane, 2007b)

We propose a method that combines linear and circular antenna to retrieve intersecting circles. We exemplify this method with an image containing two circles (see Fig. 6(a)). It falls into the following parts:

- Generate a signal on a linear antenna placed at the left and bottom sides of the image;
- Associate signal peak 1 (P1) with signal peak 3 (P3), signal peak 2 (P2) with signal peak 4 (P4);
- Diameter 1 is given by the distance P1-P3, diameter 2 is given by the distance P2-P4;
- Center 1 is given by the mid point between P1 and P3, center 2 is given by the mid point between P2 and P4;
- Associate the circular antenna with a sub-image containing center 1 and P1, perform signal generation. Check the phase linearity of the generated signal;
- Associate the circular antenna with a sub-image containing center 2 and P4, perform signal generation. Check the linearity of the generated signal.

Fig. 6(a) presents, in particular, the square sub-image to which we associate a circular antenna. Fig. 6(b) and (c) shows the generated signals.
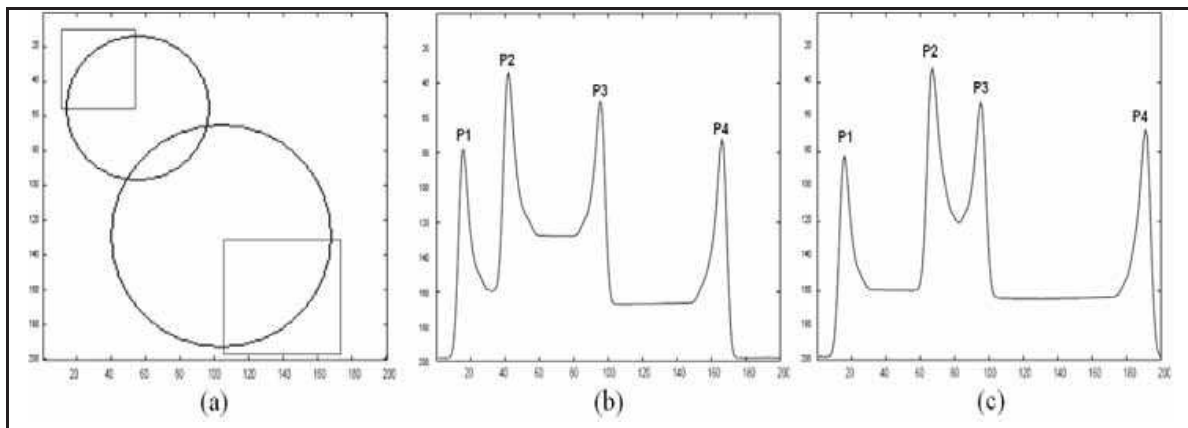
Fig. 6. (a) Two intersecting circles, sub-images containing center 1 and center 2; signals generated on (b) the bottom of the image, (c) the left side of the image.

8. Results

The proposed star-shaped contour detection method is first applied to a very distorted circle, and the results obtained are compared with those of the active contour method GVF (gradient vector flow) (Xu & Prince, 1997). The proposed multiple circle detection method is applied to several application cases: robotic vision, melanoma segmentation, circle detection in omnidirectional vision images, blood cell segmentation. In the proposed applications, we use GVF as a comparative method or as a complement to the proposed circle estimation method. The values of the parameters for GVF method (Xianghua & Mirmehdi, 2004) are the following. For the computation of the edge map: 100 iterations; $\mu_{GVF} = 0,09$ (regularization coefficient); for the snakes deformation: 100 initialization points and 50 iterations; $\alpha_{GVF} = 0.2$ (tension); $\beta_{GVF} = 0.03$ (rigidity); $\gamma_{GVF} = 1$ (regularization coefficient); $\kappa_{GVF} = 0.8$ (gradient strength coefficient). The value of the propagation parameter values for signal generation in the proposed method are $\mu = 1$ and $\alpha = 5 \ 10^{-3}$.

8.1 Hand-made images
In this subsection we first remind a major result obtained with star-shaped contours, and then proposed results obtained on intersecting circle retrieval.

8.1.1 Very distorded circles
The abilities of the proposed method to retrieve highly concave contours are illustrated in Figs. 7 and 8. We provide the mean error value over the pixel radial coordinate $M E_\rho$. We notice that this value is higher when GVF is used, as when the proposed method is used.
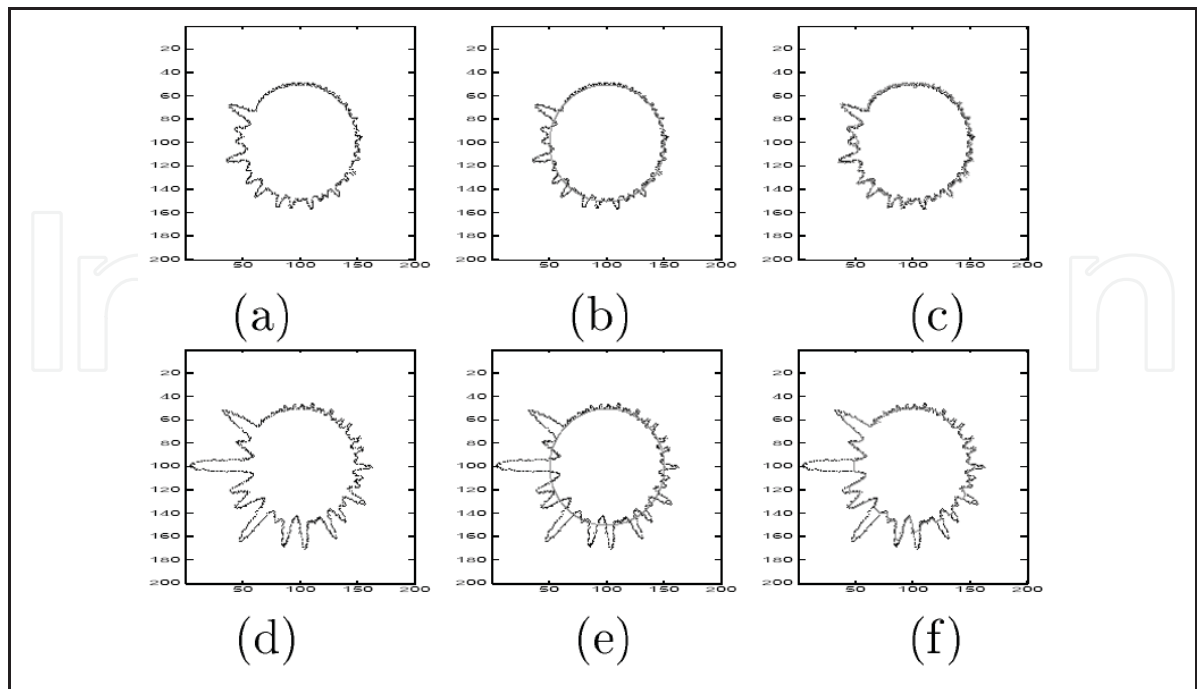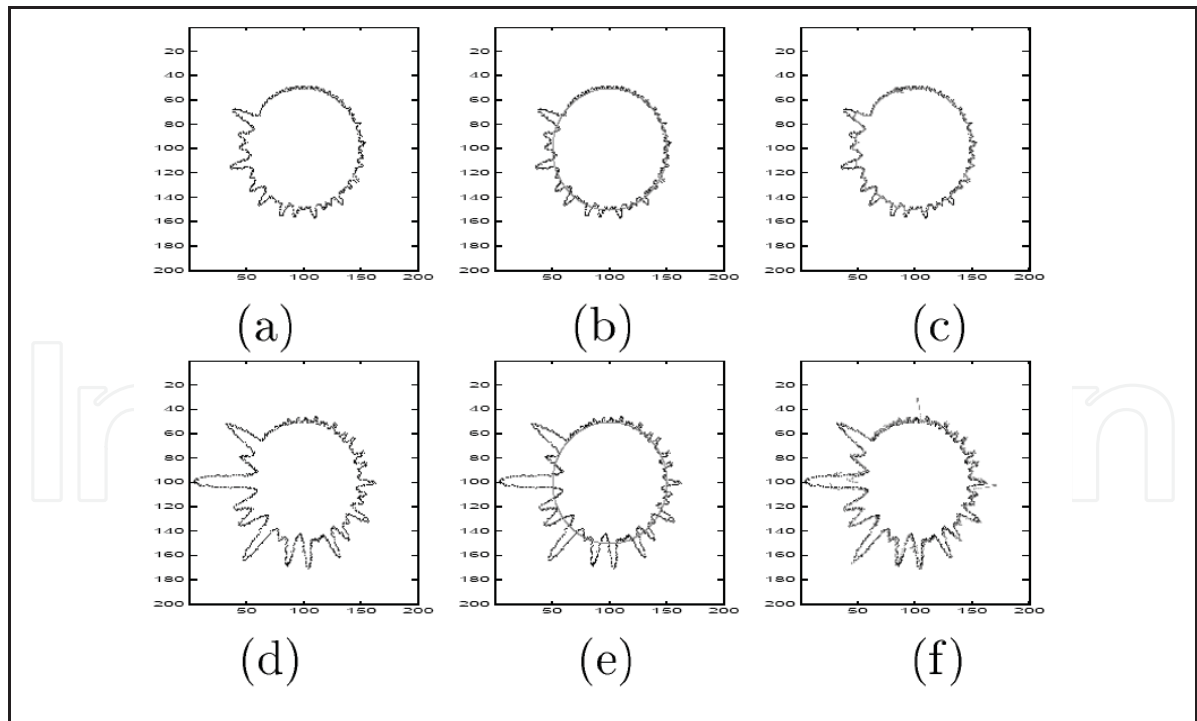
Fig. 7. Examples of processed images containing the less (a) and the most (d) distorted circles, initialization (b,e) and estimation using GVF method (c,f). ME_ρ =1.4 pixel and 4.1 pixels.

Fig. 8. Examples of processed images containing the less (a) and the most (d) distorted circles, initialization (b,e) and estimation using GVF method (c,f). ME_ρ =1.4 pixel and 2.7 pixels.

8.1.2 Intersecting circles

We first exemplify the proposed method for intersecting circle retrieval on the image of Fig. 9(a), from which we obtain the results of Fig. 9(b) and (c), which presents the signal generated on both sides of the image. The signal obtained on left side exhibits only two peak values, because the radius values are very close to each other. Therefore signal generation on linear antenna provides a rough estimate of each radius, and signal generation on circular antenna refines the estimation of both values.

The center coordinates of circles 1 and 2 are estimated as $\{l_{c1}, m_{c1}\} = \{83, 41\}$ and $\{l_{c2}, m_{c2}\} = \{83, 84\}$. Radius 1 is estimated as $r_1 = 24$, radius 2 is estimated as $r_2 = 30$.

The computationally dominant operations while running the algorithm are signal generation on linear and circular antenna. For this image and with the considered parameter values, the computational load required for each step is as follows:

- signal generation on linear antenna: $3.8\ 10^{-2}$ sec.;
- signal generation on circular antenna: $7.8\ 10^{-1}$ sec.

So the whole method lasts $8.1\ 10^{-1}$ sec. For sake of comparison, generalized Hough transform with prior knowledge of the radius of the expected circles lasts 2.6 sec. for each circle. Then it is 6.4 times longer than the proposed method.
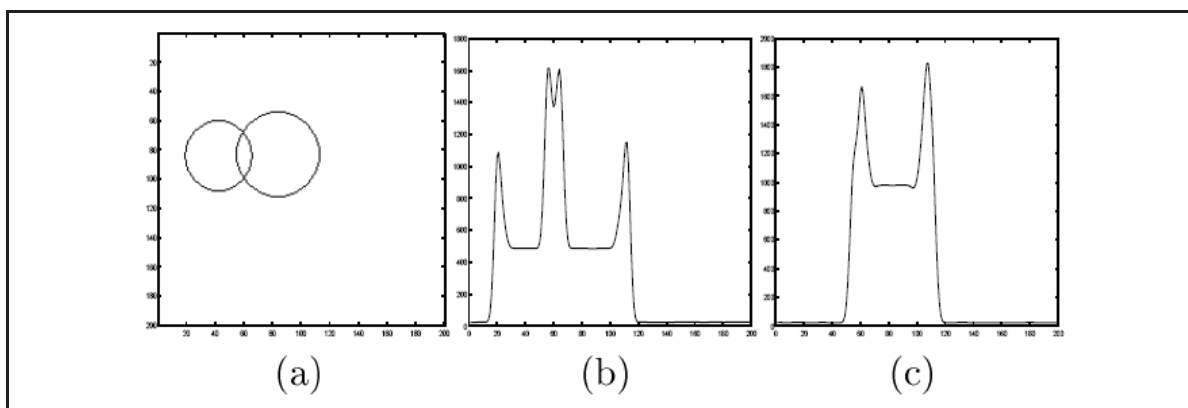
Fig. 9. (a) Processed image; signals generated on: (b) the bottom of the image; (c) the left side of the image.

The case presented in Figs. 10(a) and 10(b), (c) illustrates the need for the last two steps of the proposed algorithm. Indeed the signals generated on linear antenna present the same peak coordinates as the signals generated from the image of Fig. 7(a). However, if a subimage is selected, and the center of the circular antenna is placed such as in Fig. 7, the phase of the generated signal is not linear. Therefore, for Fig. 10(a), we take as the diameter values the distances P1-P4 and P2-P3. The center coordinates of circles 1 and 2 are estimated as $\{l_{c1}, m_{c1}\} = \{68, 55\}$ and $\{l_{c2}, m_{c2}\} = \{104, 99\}$. Radius of circle 1 is estimated as $r_1 = 87$, radius of circle 2 is estimated as $r_2 = 27$.
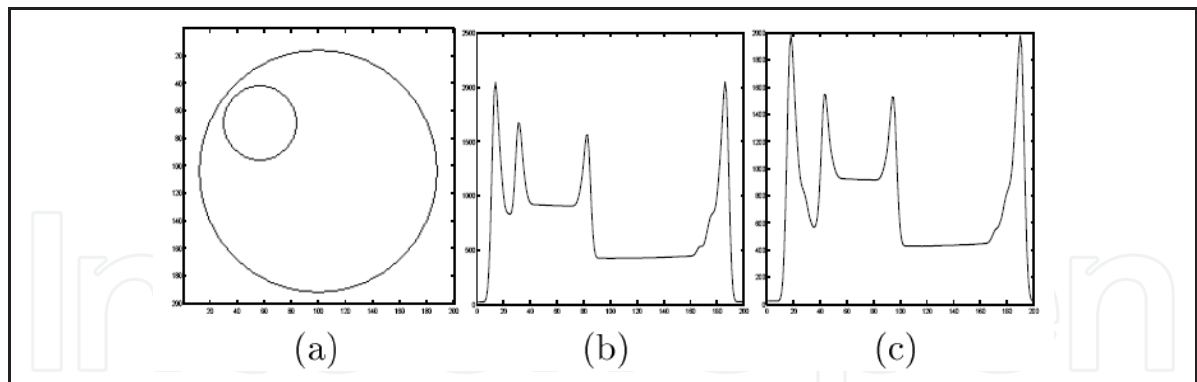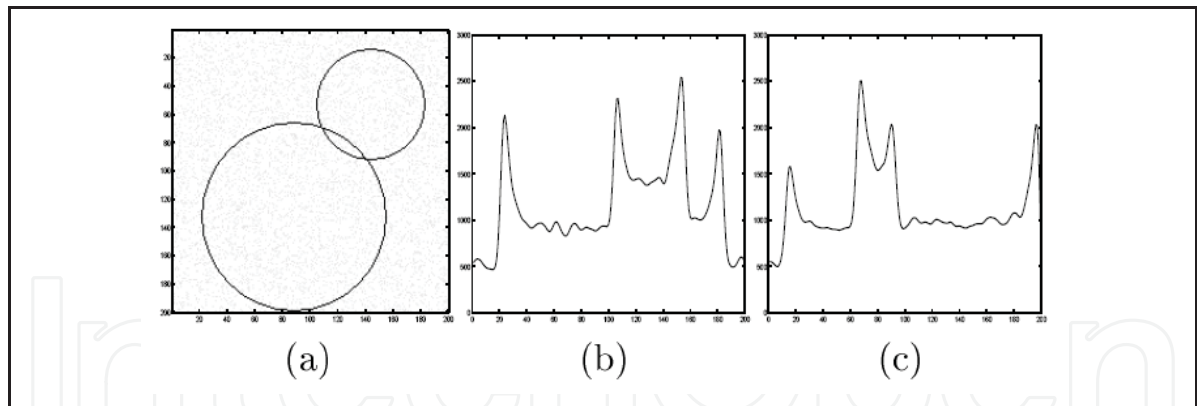
Fig. 10. (a) Processed image; signals generated on: (b) the bottom of the image; (c) the left side of the image.

Here was exemplified the ability of the circular antenna to distinguish between ambiguous cases.

Fig. 11 shows the results obtained with a noisy image. The percentage of noisy pixels is 15%, and noise grey level values follow Gaussian distribution with mean 0.1 and standard deviation 0.005. The presence of noisy pixels induces fluctuations in the generated signals, Figs. 11(b) and 11(c) show that the peaks that permit to characterize the expected circles are still dominant over the unexpected fluctuations. So the results obtained do not suffer the influence of noise pixels. The center coordinates of circles 1 and 2 are estimated as $\{l_{c1}, m_{c1}\} = \{131, 88\}$ and $\{l_{c2}, m_{c2}\} = \{53, 144\}$. Radius of circle 1 is estimated as $r_1 = 67$, radius of circle 2 is estimated as $r_2 = 40$.

Fig. 11. (a) Processed image; signals generated on: (b) the bottom of the image; (c) the left side of the image.

8.2 Robotic vision

We now consider a real-world image coming from biometrics (see Fig. 12(a)). This image contains a contour with high concavity.

Fig. 12(b) gives the result of the initialization of our optimization method. Fig. 12(c) shows that GVF fails to retrieve the furthest sections of the narrow and deep concavities of the hand, that correspond to the two right-most fingers. Fig. 12(d) shows that the proposed method for distortion estimation manages to retrieve all pixel shift values, even the elevated

ones. We also noticed that the computational time which is required to obtain this result with GVF is 25-fold higher than the computational time required by the proposed method: 400 sec. are required by GVF, and 16 sec. are required by our method.
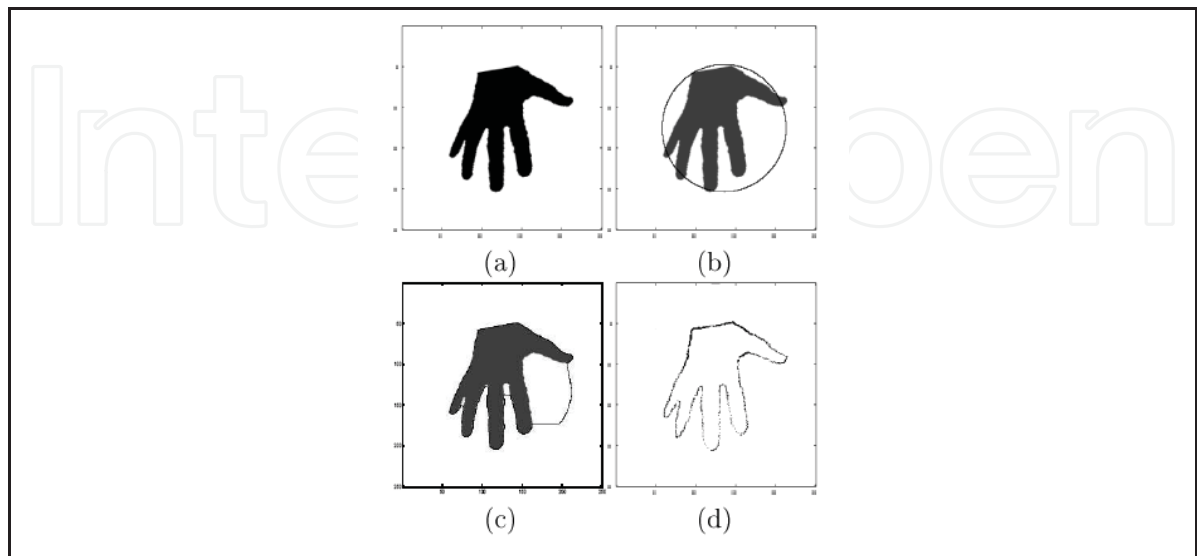

Fig. 12. Hand localization: (a) Processed image, (b) initialization, (c) final result obtained with GVF, (d) final result obtained with the proposed method

8.3 Omnidirectionnal images

Figures 13(a), (b), (c) show three omnidirectional images, obtained with a hyperbolic mirror. For some images it is useful to remove to parasite circles due to the acquisition system.

The experiment illustrated on Fig. 14 is an example of characterization of two circles that overlap. Figures 14(a), (b), (c), show for one image the gradient image, the threshold image, the signal generated on the bottom side of the image (Marot & Bourennane, 2008). The samples for which the generated signal takes none zero values (see Fig. 14(c)) delimitate the external circle of Fig. 13(a).

The diameter of the big circle is 485 pixels and the horizontal coordinate of its center is 252 pixels. This permits first to erase the external circle, secondly to characterize the intern circle by the same method.
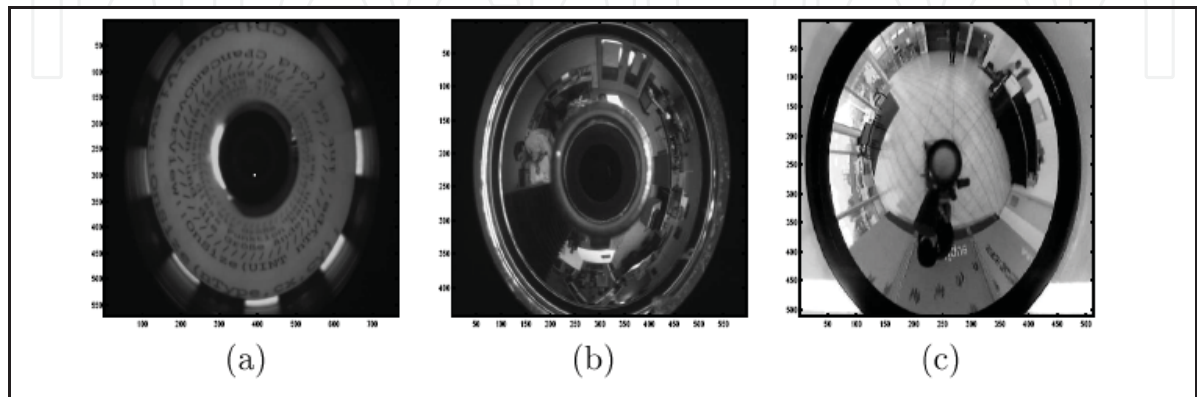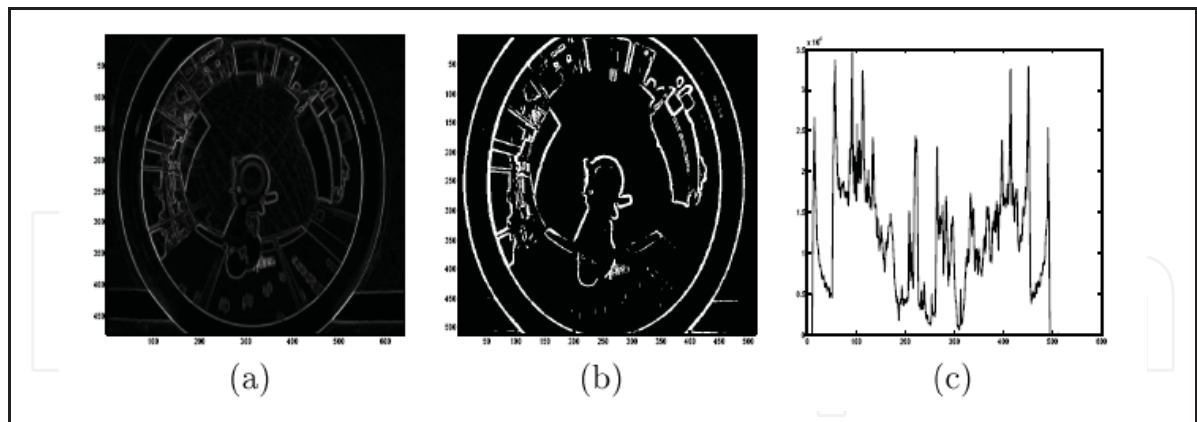

Fig. 13. Omnidirectional images

Fig. 14. Circle characterization by signal generation

8.4 Cell segmentation

Fig. 15 presents the case of a real-world image. It contains one red cell and one white cell. Our goal in this application is to detect both cells. The minimum value in the signal generated on bottom side of the image corresponds to the frontier between both cells. The width of the non-zero sections on both sides of the minimum value is the diameter of each cell. Each peak value in each generated signal provides one center coordinate.
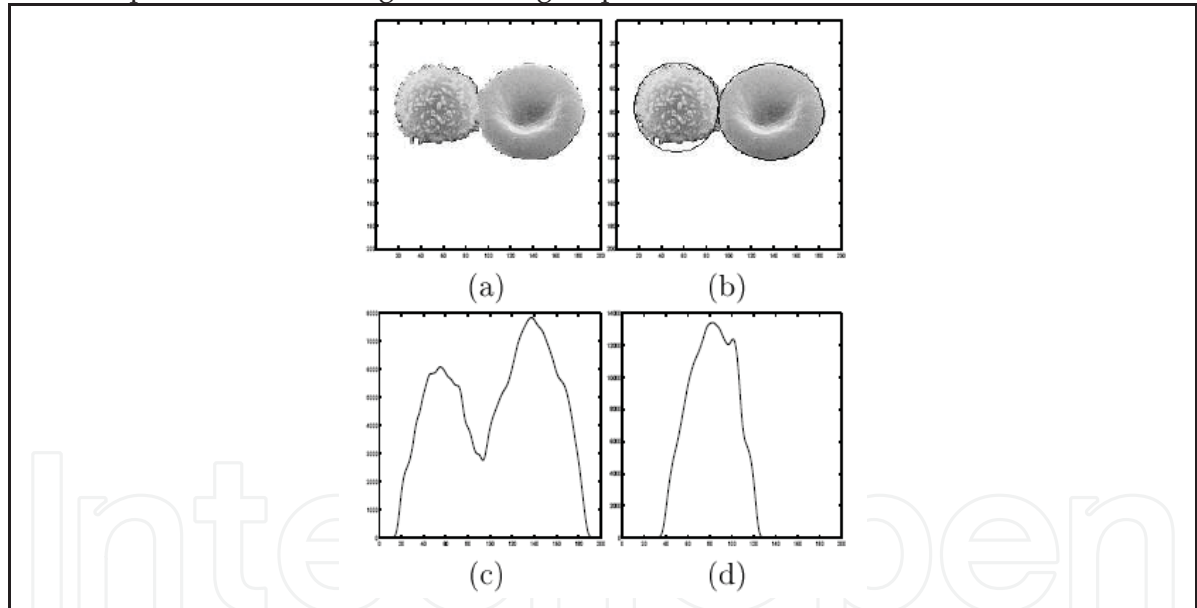

Fig. 15. Blood cells: (a) processed image; (b) superposition processed image and result; signals generated on: (c) the bottom of the image; (d) the left side of the image.

8.5 Melanoma segmentation

Fig. 16 concerns quantitative analysis in a medical application. More precisely, the purpose of the experiment is to detect the frontier of a melanoma. The melanoma was chosen randomly out of a database (Stolz et al., 2003).
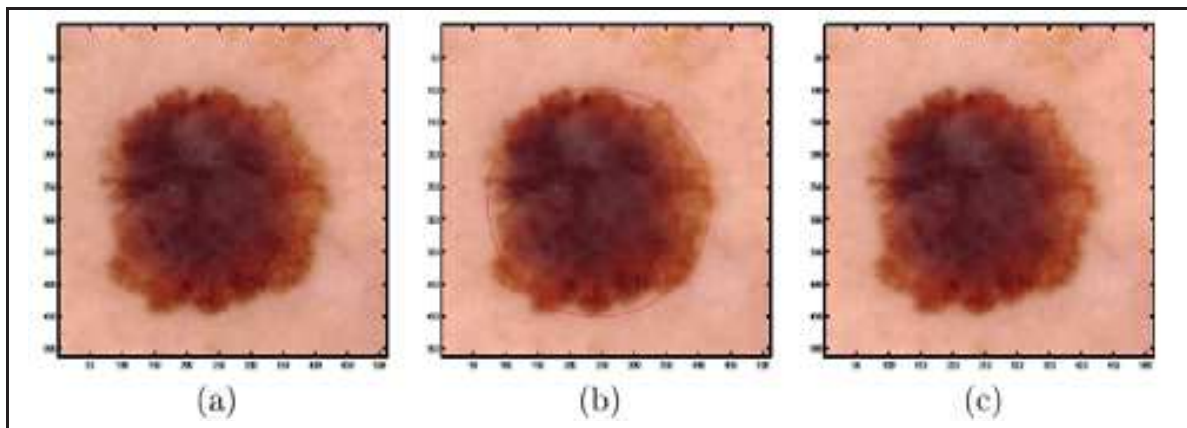
Fig. 16. Melanoma segmentation: (a) processed image, (b) elliptic approximation by the proposed array processing method, (c) result obtained by GVF.

The proposed array processing method detects a circular approximation of the melanoma borders (Marot & Bourennane, 2007b; Marot & Bourennane, 2008) (see Fig 16(b)). A few iterations of GVF method (Xu & Prince, 1997) yield the contour of the melanoma (see Fig 16(c)). Such a method can be used to control automatically the evolution of the surface of the melanoma.

9. Conclusion

This chapter deals with contour retrieval in images. We review the formulation and resolution of rectilinear or circular contour estimation. The estimation of the parameters of rectilinear or circular contours is transposed as a source localization problem in array processing. We presented the principles of SLIDE algorithm for the estimation of rectilinear contours based on signal generation upon a linear antenna. In this frame, high-resolution methods of array processing retrieve possibly close parameters of straight lines in images. We explained the principles of signal generation upon a virtual circular antenna. The circular antenna permits to generate linear phase signals out of an image containing circular features. The same signal models as for straight line estimation are obtained, so high-resolution methods of array processing retrieve possibly close radius values of concentric circles. For the estimation of distorted contours, we adopted the same conventions for signal generation, that is, either a linear or a circular antenna. For the first time, in this book chapter, we propose an intersecting circle retrieval method, based on array processing algorithms. Signal generation on a linear antenna yields the center coordinates and radii of all circles. Circular antenna refines the estimation of the radii and distinguishes ambiguous cases. The proposed star-shaped contour estimation method retrieves contours with high concavities, thus providing a solution to Snakes based methods. The proposed multiple circle estimation method retrieves intersecting circles, thus providing a solution to levelset-type methods. We exemplified the proposed method on hand-made and real-world images. Further topics to be studied are the robustness to various types of noise, such as correlated Gaussian noise.

10. References

Abed-Meraim, K. & Hua, Y. (1997). Multi-line fitting and straight edge detection using polynomial phase signals, *ASILOMAR31*, Vol. 2, pp. 1720-1724, 1997.

Aghajan, H. K. & Kailath, T. (1992). A subspace Fitting Approach to Super Resolution Multi-Line Fitting and Straight Edge Detection, *Proc. of IEEE ICASSP*, vol. 3, pp. 121-124, 1992.

Aghajan, H. K. & Kailath, T. (1993a). Sensor array processing techniques for super resolution multi-line-fitting and straight edge detection, *IEEE Trans. on IP*, Vol. 2, No. 4, pp. 454-465, Oct. 1993.

Aghajan, H.K. & Kailath, T. (1993b). SLIDE: subspace-based line detection, *IEEE int. conf. ASSP*, Vol. 5, pp. 89 - 92, April 27-30, 1993.

Aghajan, H. & Kailath, T. (1995). SLIDE: Subspace-based Line detection, *IEEE Trans. on PAMI*, 16(11):1057-1073, Nov. 1994.

Aghajan, H.K. (1995). Subspace Techniques for Image Understanding and Computer Vision, PhD Thesis, Stanford University, 1995

Bourennane, S. & Marot, J. (2005). Line parameters estimation by array processing methods, *IEEE ICASSP*, Vol. 4, pp. 965-968, Philadelphie, Mar. 2005.

Bourennane, S. & Marot, J. (2006a). Estimation of straight line offsets by a high resolution method, *IEE proceedings - Vision, Image and Signal Processing*, Vol. 153, issue 2, pp. 224-229, 6 April 2006.

Bourennane, S. & Marot, J. (2006b). Optimization and interpolation for distorted contour estimation, *IEEE-ICASSP*, vol. 2, pp. 717-720, Toulouse, France, April 2006.

Bourennane, S. & Marot, J. (2006c). Contour estimation by array processing methods, *Applied signal processing*, article ID 95634, 15 pages, 2006.

Bourennane, S.; Fossati, C. & Marot, J., (2008). About noneigenvector source localization methods *EURASIP Journal on Advances in Signal Processing* Vol. 2008, Article ID 480835, 13 pages doi:10.1155/2008/480835

Brigger, P. ; Hoeg, J. & Unser, M. (2000). B-Spline Snakes: A Flexible Tool for Parametric Contour Detection, *IEEE Trans. on IP*, vol. 9, No. 9, pp. 1484-96, 2000.

Cheng, J. & Foo, S. W. (2006). Dynamic directional gradient vector flow for snakes, *IEEE Trans. on Image Processing*, vol. 15, no. 6, pp.1563-1571, June 2006.

Connell, S. D. & Jain, A. K. (2001). Template-based online character recognition, *Pattern Rec.*, vol. 34, no 1, pp: 1-14, 2001.

Gander, W.; Golub, G.H. & Strebel, R. (1994). Least-squares fitting of circles and ellipses , *BIT*, n. 34, pp. 558-578, 1994.

Halder, B. ; Aghajan, H. & T. Kailath (1995). Propagation diversity enhancement to the subspace-based line detection algorithm, *Proc. SPIE Nonlinear Image Processing VI* Vol. 2424, p. 320-328, pp. 320-328, March 1995.

Jones, D.R. ; Pertunen, C.D. & Stuckman, B.E. (1993). Lipschitzian optimization without the Lipschitz constant, *Journal of Optimization and Applications*, vol. 79, no. 157-181, 1993.

Karoui, I.; Fablet, R.; Boucher, J.-M. & Augustin, J.-M. (2006). Region-based segmentation using texture statistics and level-set methods, *IEEE ICASSP*, pp. 693-696, 2006.

Kass, M.; Witkin, A. & Terzopoulos, D. (1998). Snakes: Active Contour Model, *Int. J. of Comp. Vis.*, pp.321-331, 1988

Kiryati, N. & Bruckstein, A.M. (1992). What's in a set of points? [straight line fitting], *IEEE Trans. on PAMI*, Vol. 14, No. 4, pp.496-500, April 1992.

Marot, J. & Bourennane, S. (2007a). Array processing and fast Optimization Algorithms for Distorted Circular Contour Retrieval , *EURASIP Journal on Advances in Signal Processing*, Vol. 2007, article ID 57354, 13 pages, 2007.

Marot, J. & Bourennane, S. (2007b). Subspace-Based and DIRECT Algorithms for Distorted Circular Contour Estimation, *IEEE Trans. On Image Processing*, Vol. 16, No. 9, pp. 2369-2378, sept. 2007.

Marot, J., Bourennane, S. & Adel, M. (2007). Array processing approach for object segmentation in images, *IEEE ICASSP'07*, Vol. 1, pp. 621-24, April 2007.

Marot, J. & Bourennane, S. (2008). Array processing for intersecting circle retrieval, *EUSIPCO'08*, 5 pages, Aug. 2008.

Marot, J.; Fossati, C.; & Bourennane, S. (2008) Fast subspace-based source localization methods *IEEE-Sensor array multichannel signal processing workshop*, Darmstadt Germany, 07/ 2008

Osher, S. & Sethian, J. (1998). Fronts propagating with curvature-dependent speed: algorithms based on Hamilton-Jacobi formulations, *J. Comput. Phys.* , Vol. 79, pp. 12-49, 1988.

Paragios, N. & Deriche, R. (2002). Geodesic Active Regions and Level Set Methods for Supervised Texture Segmentation, *Int'l Journal of Computer Vision*, Vol. 46, No 3, pp. 223-247, Feb. 2002.

Pillai, S.U. & Kwon, B.H. (1989). Forward/backward spatial smoothing techniques for coherent signal identification, *Proc. of IEEE trans. on ASSP*, vol. 37 (1), pp. 8-15, 1989.

Precioso, F. ; Barlaud, M. ; Blu, T. & Unser, M. (2005). Robust Real-Time Segmentation of Images and Videos Using a Smooth-Spline Snake-Based Algorithm, *IEEE Trans. on IP*, Vol. 14, No. 7, pp. 910-924, July 2005.

Roy, R. & Kailath, T. (1989). ESPRIT: Estimation of signal parameters via rotational invariance techniques, *IEEE Trans. on ASSP*, vol. 37, no. 7, pp. 984-995, 1989.

Sheinvald, J. & Kiryati,N. (1997). On the Magic of SLIDE, *Machine Vision and Applications*, Vol. 9, pp. 251-261, 1997.

Stolz, W. ; Horsch, A. ; Pompl, R. ; Abmayr, W. ; Landthaler, M. (2003) Datensatz Dermatology Skin Surface Microscopy Melanocytic Lesions 749, Version 1.0, October 2003 (D-SSM-ML-749 V1.0).

Tufts, D.W. & Kumaresan, R. (1982). Estimation of frequencies of multiple sinusoids: making linear prediction perform like maximum likelihood, *Proc. IEEE*, vol. 70, pp. 975-989, sept. 1982.

Unser, M. ; Aldroubi, A. & Eden, M. (1993). B-spline signal processing: Part I-theory; part II-efficient design and applications, *IEEE Trans. on SP*, Vol. 41, No. 2, pp. 821-848, Feb. 1993.

Xianghua X. & Mirmehdi, M. (2004). RAGS: region-aided geometric snake , *IEEE Trans. IP*, Vol. 13, no. 5, pp: 640-652, May 2004.

Xu, C. & Prince, J.L. (1997). Gradient vector flow: a new external force for snakes, *Proceeding of IEEE Computer Society Conference on Computer -Vision and Pattern Recognition* pp. 66-71, Jun. 1997.

Zhu, S. C. & Yuille, A. (1996). Region Competition: Unifying Snakes, Region Growing, and Bayes /MDL for Multiband Image Segmentation, *IEEE Trans. on PAMI*, Vol. 18, No. 9, pp. 884-900, Sept. 1996.
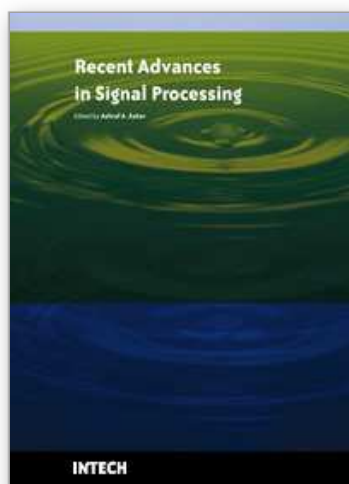
Recent Advances in Signal Processing

Edited by Ashraf A Zaher

The signal processing task is a very critical issue in the majority of new technological inventions and challenges in a variety of applications in both science and engineering fields. Classical signal processing techniques have largely worked with mathematical models that are linear, local, stationary, and Gaussian. They have always favored closed-form tractability over real-world accuracy. These constraints were imposed by the lack of powerful computing tools. During the last few decades, signal processing theories, developments, and applications have matured rapidly and now include tools from many areas of mathematics, computer science, physics, and engineering. This book is targeted primarily toward both students and researchers who want to be exposed to a wide variety of signal processing techniques and algorithms. It includes 27 chapters that can be categorized into five different areas depending on the application at hand. These five categories are ordered to address image processing, speech processing, communication systems, time-series analysis, and educational packages respectively. The book has the advantage of providing a collection of applications that are completely independent and self-contained; thus, the interested reader can choose any chapter and skip to another without losing continuity.

How to reference

In order to correctly reference this scholarly work, feel free to copy and paste the following:

J. Marot, C. Fossati and Y. Caulier (2009). About Array Processing Methods for Image Segmentation, Recent Advances in Signal Processing, Ashraf A Zaher (Ed.), ISBN: 978-953-307-002-5, InTech, Available from: http://www.intechopen.com/books/recent-advances-in-signal-processing/about-array-processing-methods-for-image-segmentation

INTECH
open science | open minds